*Desalination and Water Treatment*
www.deswater.com

doi: 10.5004/dwt.2021.27383

229 (2021) 134–144
July

# Nitrate removal from aqueous solution by activated carbon prepared from shrimp shell

Weiliang Pan[a,†], Rui Deng[a,*,†], Yunpeng Cao[a], Fan Xia[b], Qiye Wu[a], Li Gu[c]

[a]*Chongqing Jiaotong University, Chongqing, 69 Xuefu Avenue, Chongqing 400074, China, email: 21260091@qq.com (R. Deng)*
[b]*China Railway Construction Real Estate Group (East China) Co., Ltd., Room 202, Building 16, Shuangwan International City, Gongshu District, Hangzhou City, Zhejiang Province, Zhejiang 200070, China*
[c]*Key laboratory of the Three Gorges Reservoir Region's Eco-environments, Ministry of Education, College of Environment and Ecology, Chongqing University, 174 Shapingba Road, Chongqing 400045, China*

Received 17 November 2020; Accepted 15 April 2021

**ABSTRACT**

In this study, activated carbon was prepared after pyrolysis and activation of shrimp shells. The effects of different impregnation ratios and temperatures on the physical and chemical properties of activated carbon were investigated. The physical and chemical properties of different activated carbons were characterized by $N_2$ adsorption–desorption, scanning electron microscopy, and X-ray diffraction. The results show that at a pyrolysis temperature of 400°C, the activated carbon with a C/$ZnCl_2$ ratio of 1/2 has the maximum specific surface area and pore volume of 1,536.3 $m^2/g$ and 0.83 $cm^3/g$, respectively. The experimental results show that with the increase of pH value, the adsorption capacity of activated carbon will gradually decrease, indicating that acidic conditions are more favorable for nitrate adsorption. The maximum adsorption capacity was of the carbon achieved at about 5.58 mg/g at such conditions. The pseudo-first-order kinetic model fits well with the nitrate adsorption kinetics date with a high determination coefficient ($R^2 > 0.95$), while both the Freundlich and Langmuir isothermal model fit the experimental data well ($R^2 > 0.95$). Also, the influence of the coexisting anions on the adsorption performance of activated carbon has also been studied, the inhibitory effect of coexisting anions on the adsorption of nitrate on activated carbon is from high to low: $CO_3^{2-} > SO_4^{2-} > Cl^-$.

*Keywords:* Activated carbon; Shrimp shell; Nitrate; Adsorption

## 1. Introduction

With the acceleration of urbanization and the rapid development of industry, a large number of water bodies have been polluted [1]. Nitrate nitrogen in groundwater mainly comes from the use of various types of agricultural chemical fertilizers, domestic sewage, animal excrement, etc. [2,3]. It will cause eutrophication of water and the proliferation of algae, thus affecting the environment [4]. The high concentration level of nitrate in drinking water may be converted into nitrite after being ingested by the human body, which could cause methemoglobinemia, especially for babies [5–9]. Therefore, the World Health Organization (WHO) allows concentrations of nitrate in groundwater and drinking water to be 50 and 10 mg/L ($NO_3^-$–N) [10].

In order to remove the nitrates from the water, different types of technologies have been developed. These technologies can be mainly divided into biological denitrification and physical–chemical reduction technologies [11]. Biological technologies commonly present low operating costs, but it is susceptible to blockage and temperature due to the sensitivity of microorganisms [12,13]. Additional carbon sources

* Corresponding author.

† These authors contributed equally to this work.

are generally required as nutrients when high denitrification efficiency is needed. Chemical reduction methods remove nitrate from water by adding a reducing agent [14]. Active metal, hydrogen, formic acid, and methanol are commonly used as reducing agents. This method commonly presents a high reaction rate, but it also produces additional by-products and requires accurate operational conditions. Physical-chemical methods include adsorption [15], ion exchange [16], reverse osmosis [17], and membrane separation [18]. In these methods, the adsorption method shows some superiority due to its high efficiency and simple operation, the adsorption has been proved to be one of the most effective methods to remove all kinds of pollutants from wastewater [19–21]. In nitrate removal, various adsorbents have been adopted, including clay-derived materials, polymer-derived materials, and carbon-derived materials. Among them, carbon-derived materials, including activated carbon, biochar, as well as graphene, have attracted wide attention due to their wide variety, low cost, and easy availability [22].

Recently, biochar prepared under oxygen-limited conditions has become a hot issue due to its low production cost and simple preparation process and can be used as an adsorbent to remove pollutants in water [23,24]. However, the crude biochar produced is directly used as an adsorbent, the effect is not good. It is necessary to modify the internal and morphology of biochar through activation to obtain better performance. According to literature reports, compared with the physical activity method, activated carbon prepared by the activated activation method has the advantages of larger specific surface area and less time consumption [25,26]. In the activation process, the activator plays an important role in the formation of activated carbon pores, as dehydrating agent role, reducing tar and other liquid materials in the process of activation, prompting volatile substances can be more smoothly through the pore, and not cause pore blockage, which can promote the activated carbon to form more holes [27]. Using zinc chloride as the activator, the biochar obtained by pyrolysis of safflower seed cake was activated by the chemical activation method. The activated carbon had an adsorption capacity of 128.21 mg/g for methyl blue under optimal conditions [28]. The surface area of rice husk biochar activated by zinc chloride at a ratio of 3:1 for 1 h was 645 $m^2/g$, which was higher than that of non-activated biochar (28 $m^2/g$) [29]. These activated carbon have been widely used in removing different kinds of pollutants in water including heavy metal ions, synthetic dyes, nitrate, phosphate, and others [30–32]. Nowadays, preparing carbon by using natural chitin has attracted attention. Chitin is quite abundant in the natural environment, mainly as waste material from a fishery, which contains a lot of carbon and rich functional groups [33,34]. Shrimp shell is a nitrogen-rich carbon material rich in protein and chitin in fisheries and can be used to prepare porous carbon [35]. Magnacca et al. [36] prepared biochar by using chitin for energetic and environmental applications, and the results indicated that the surface area of the biochars was about 330 $m^2/g$. Xiao et al. [37] used shrimp shell under high temperature and oxygen restriction conditions, to adsorb heavy metal ions in water, the experimental results showed that shrimp shell biochar had a good removal rate for Pb(II), and its high adsorption capacity was related to its physical properties [30]. Despite the above research, the preparation of chitin-derived biochar and its use as an adsorbent to remove nitrate from water are still lacking. Shrimp shells are used as waste in fishery industries, and the total product amount in China is about 1.27 million t/y. So, it is of great economic and environmental significance to prepare carbo from shrimp shells through solid waste reduction and innocuity recycling effective utilization.

According to the literature, the properties of activated carbon depend on not only the carbonization temperature but also the activation procedure [22]. The increase of the carbonization temperature commonly leads to the diffusion of volatile substances on the surface, resulting in more pore space. In the procedure of activation, different kinds of activators play different roles in shaping porous structures of the activated carbon [26]. The most used activators include sodium hydroxide of zinc chloride and orthophosphoric acid. They are all reported to pose positive effects in promoting the porous structures, which would show a close relationship with activated carbon adsorption properties [38].

Based upon the analysis, this work aimed to evaluate the potential of shrimp shells to produce activated carbon, using a simple pyrolysis and activation process, and apply the activated carbon to remove nitrate from water. The shrimp shell-derived activated carbon was prepared and characterized. The potential of the activated carbon as an adsorbent to adsorb nitrate from the water was extensively evaluated. For this purpose, the factors affecting the process of adsorption were evaluated. Kinetic and equilibrium studies were carried out to understand the adsorption mechanism.

## 2. Materials and methods

### 2.1. Materials and reagents

Shrimp shell was obtained from the waste of an aquatic product sales market located in Chongqing city. Samples were washed several times by using deionized water. Then the sample was dried at 105°C for 8 h, followed by grinding. Particles were sieved and the particles lower than 100 mesh were selected for the biochar preparation. All chemicals and reagents used in this study were of analytical grades, and the chemical solutions were prepared using deionized (DI) water. Zinc chloride ($ZnCl_2$), sodium chloride (NaCl), Hydrochloric acid (HCl), and sodium hydroxide (NaOH) were purchased from China Chemicals Inc., (Beijing, China). Sodium salts of nitrate, sulfates, chloride, phosphate, and carbonate were purchased from Dingshengxin Chemical Industry Co., Ltd., (Tianjin, China).

### 2.2. Preparation of different activated carbons

Shrimp shell-derived activated carbon was prepared through the processes of pyrolysis and activation. A quartz reactor was placed in a tube furnace (Shanghai Yifeng Laboratory Instrument Co., Shanghai, China) under an $N_2$ atmosphere. The heater temperature was increased at a rate of 5°C/min until 400 (C-400) or 600°C (C-600), being held at the end temperature for 120 min and allowed to cool still under $N_2$ flow until room temperature. Activated carbon

used in this work were prepared by the $ZnCl_2$ activation method that the shrimp shell particles are pre-impregnated into 300 mL of a 40% $ZnCl_2$ solution with the C/$ZnCl_2$ ratio of 1/1 or 1/2 (C-400-1 means the biochar prepared in 400°C with the C/$ZnCl_2$ ratio of 1/1, which C-600-2 means the biochar prepared in 600°C with the C/$ZnCl_2$ ratio of 1/2) before the procedure of pyrolysis. The pyrolyzed mixtures were rinsed with distilled water several times and then dried in an oven at 105°C for approximately 24 h. Then, the samples, now referred to as activated carbons, were stored in a desiccator until further analysis.

### 2.3. Adsorption experiments

The studies were conducted by using the "bottle point" procedure. 2.5 g/L biochar activated carbon was added into 250 mL nitrate solution with different concentrations (10–150 mg/L) at specified pH conditions. The mixed solution is shaken in an Erlenmeyer flask at a temperature of 25°C for a certain contact time (SKY-211B shaker incubator, China). After the process, the solutions were taken out for analysis. After the sample was filtered by a 0.45 μm pore-sized membrane, it was used for experimental analysis. The pH of the solution was adjusted by adding 0.1 M HCl or NaOH solution. Nitrate removal percentage was calculated as follows:

$$R_{\text{nitrate}}(\%) = \frac{C_0 - C_e}{m} \times 100 \quad (1)$$

where $C_0$ and $C_e$ are the initial and equilibrium nitrate concentrations in the solutions, respectively. Each experiment was triplicated to determine the reproducibility of the measurements and the average values are reported.

The amount of nitrate adsorbed per unit weight of adsorbent ($q_e$ in mg/g) was calculated as follows:

$$q_e = \frac{(C_0 - C_e)}{m} V \quad (2)$$

where $C_0$ and $C_e$ (mg/L) are the initial and equilibrium concentrations of nitrate ions in solutions, $m$ is the mass of the adsorbent (g), and $V$ is the volume of the solution (L).

### 2.4. Analysis

According to the Standard Methods for the Examination of Water and Wastewater (American Public Health Association), $NO_3^-$–N were determined colorimetrically using a UV-vis spectrophotometer (DR-9000, HACH, USA) [15]. pH was measured using a PHS-3C pH-meter, respectively. The porous structure of the samples, including the surface area ($S_{BET}$), the total pore volume ($V_{tot}$), and the average pore diameter. were determined from nitrogen adsorption/desorption isotherms at 77 K by using a surface area analyzer (BELSORP-mini). Field emission-scanning electron microscopy (FE-SEM, JSM-7800 F) was used to observe surface structures of different activated carbons. The X-ray diffraction (XRD) test uses the ESCALAB250Xi X-ray diffractometer from Thermo Fisher Scientific (China) Co., Ltd. The analysis conditions are working conditions: ceramic copper target X-ray tube, 40 kV voltage, 30 mA current, the scanning angle range of 5°–80°, the scanning step length of 0.02° and integration time of each step is 0.2 s.

## 3. Results and discussion

### 3.1. Characterization of different adsorbent

#### 3.1.1. Specific surface area and porous parameters

$N_2$ adsorption–desorption isotherms of different carbon adsorbents were conducted to understand their porous structures under different pyrolysis temperatures and activation conditions. According to the International Union of Pure and Applied Chemistry (IUPAC), it can be seen from Fig. 1 that the $N_2$ adsorption–desorption isotherms of unactivated carbon (C-400) and activated carbon (C-600-1, C-600-2) are similar to the type IV, $H_4$ hysteresis loop of IUPAC classification. With the increase of relative pressure, the adsorption capacity of adsorbent for nitrogen increased rapidly, indicating that there are a large number of micropores in activated carbon.

From Fig. 2, It can be seen from Fig. 2 that the pore structure of biochar (C-400) presents a multimodal distribution, mainly mesopores, and the activated carbon after activation is mainly micropores. The increase of activation temperature promotes the overall pore size to shrink, and the increase in impregnation ratio can promote the appearance of more micropores. The results of specific surface area and porous parameters are shown in Table 1. Main porous parameters including BET surface area ($S_{BET}$), total pore volume ($V_t$), average pore radius ($R_p$), and the surface area of micropores, which can be obtained from the isotherms presented in Table 1.

From Table 1, the biochars without the procedure of activation under different pyrolysis temperatures (400°C and 600°C) show close porous properties. There were low $S_{BET}$ of them with the value of 11.9 and 45.8 $m^2/g$ without significant microporous structures. These results are quite accordant to the previous studies that the directly pyrolyzed biochar commonly presented limited porous structures. It should be noticed from the table that the activation process enriched the porous structure of the biochar significantly. For the biochar activated by using the C/$ZnCl_2$ ratio of 1/1, the $S_{BET}$ can be increased from 11.9 to 496.9 $m^2/g$ for the sample pyrolyzed at 400°C, while that increased from 45.8 to 773.5 $m^2/g$ for the samples prepared at 600°C. The increase of the $ZnCl_2$ content in the activation process further improved the $S_{BET}$ to 1,536.3 and 1,177.7 $m^2/g$ for the samples prepared at 400°C and 600°C, respectively. It should be notice that the process of activation mainly enlarges the volumes and the surface areas of micropores. With the increase of the $S_{BET}$ and $S_{micro}$, the parameters of $V_t$, $V_{micro}$, and $S_{micro}$ increase, while the indexes of $V_{meso}$, as well as $R_p$, were decreased. The $R_p$ can be used to reflect the pore size distribution. The $R_p$ for directly pyrolyzed biochar at the temperature of 400°C and 600°C are 27.8 and 11.2 nm, indicating that the mesopore dominates in the biochar. The activation process turns things around, and the active ones present adequate microporous structures with the $V_p$ ranging from 0.63 to 1.21 nm. Due to the close relationship

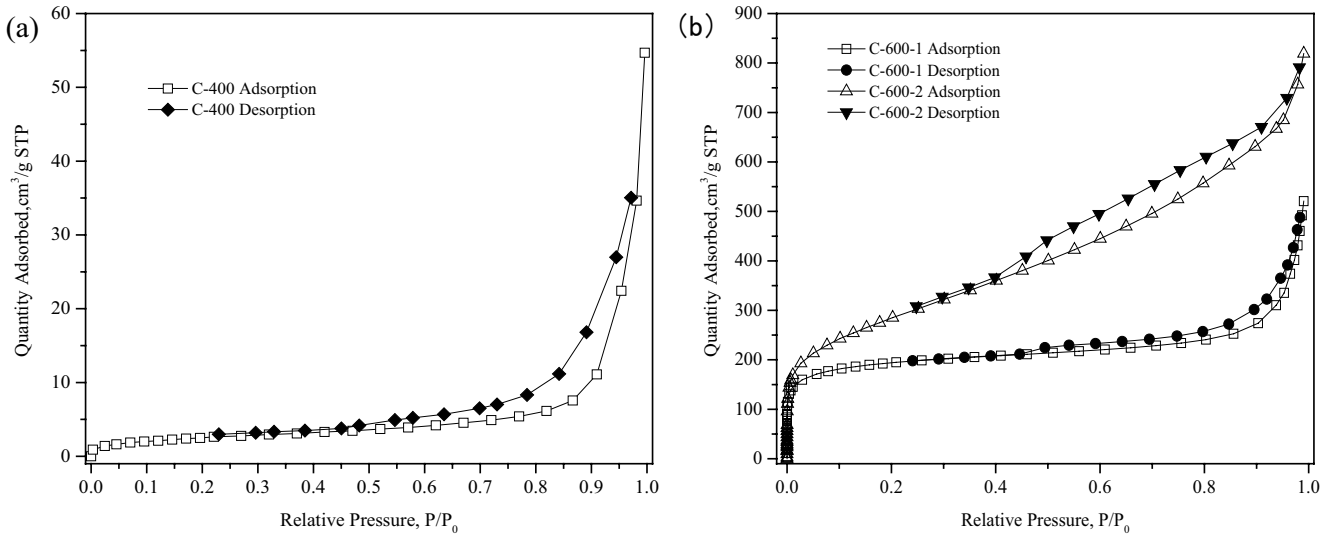


Fig. 1. Isothermal adsorption line of shrimp shell biochar and activated carbon: (a) C-400 and (b) shrimp shell activated carbon under different activation conditions.

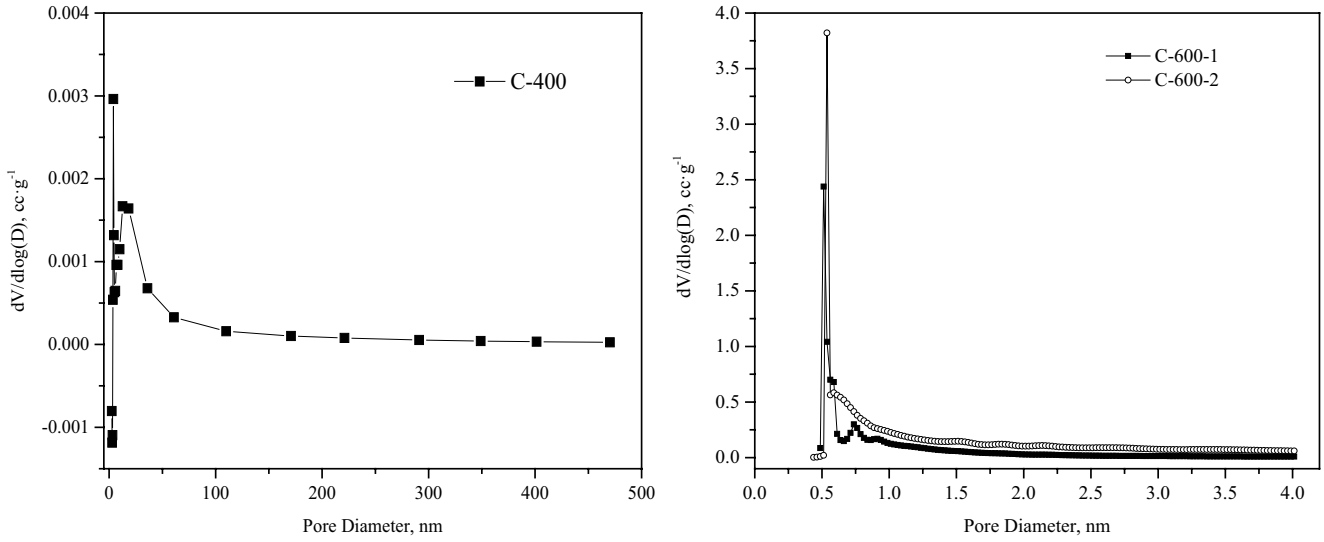


Fig. 2. Pore size distribution diagram of shrimp shell biochar and activated carbon.

Table 1
Specific surface area and porous parameters of shrimp shell biochar

| | C-400 | C-400-1 | C-400-2 | C-600 | C-600-1 | C-600-2 |
|---|---|---|---|---|---|---|
| $S_{BET}$ (m²/g) | 11.9 | 496.9 | 1,536.3 | 45.8 | 773.5 | 1,177.7 |
| $V_t$ (cm³/g) | 0.08 | 0.20 | 0.83 | 0.12 | 0.29 | 0.58 |
| $S_{micro}$ (m²/g) | / | 524.5 | 1,506.5 | / | 751.2 | 1,062.1 |
| $V_{micro}$ (cm³/g) | / | 0.18 | 0.55 | / | 0.26 | 0.42 |
| $V_{meso}$ (cm³/g) | 0.08 | 0.03 | 0.29 | 0.14 | 0.034 | 0.16 |
| $R_p$ (nm) | 27.8 | 0.63 | 1.21 | 11.2 | 0.75 | 0.98 |

between adsorption capacity and the surficial properties, the sufficient microporous structures of this activated carbon indicate that these activated carbons may present a good affinity towards target pollutants.

*3.1.2. Surface morphology*

The surface morphology of different shrimp shell-based activated carbons were studied by using scanning electron microscopy (SEM), and the results are shown in Fig. 3. From Fig. 3, we can see that the outer surface of the raw shrimp shell is smooth with regular stripes. Direct pyrolysis can hardly change the surface morphology, and the SEM results for the sample pyrolyzed at 400°C without activation (C-400) are close to that of the raw shrimp shell. The surfaces of activated biochars were significantly different from the non-activated ones, which was mainly due to the activation effects brought by $ZnCl_2$ addition. The results for sample C400-1 and C600-1 shown in Table 1 present the evidence that porous structures, especially the microporous structures were fully developed by the method of activation. Besides, there is no significant difference in surface morphology among the activated carbons pyrolyzed at different temperatures under the same activation condition (C400-1 and C600-1). However, compared to the sample of C400-1, some small solid particles attached to the surface of the sample C600-1, indicating that more ash was formed at a higher pyrolysis temperature.

*3.1.3. X-ray diffraction*

XRD patterns of different carbon samples including C-400, C-400-1, and C-600-1 are shown in Fig. 4. It can be seen from the figure that the main components of shrimp shell carbon are $CaCO_3$, and they are mainly found in calcite and aragonite. In the XRD pattern of C-400, the peak at

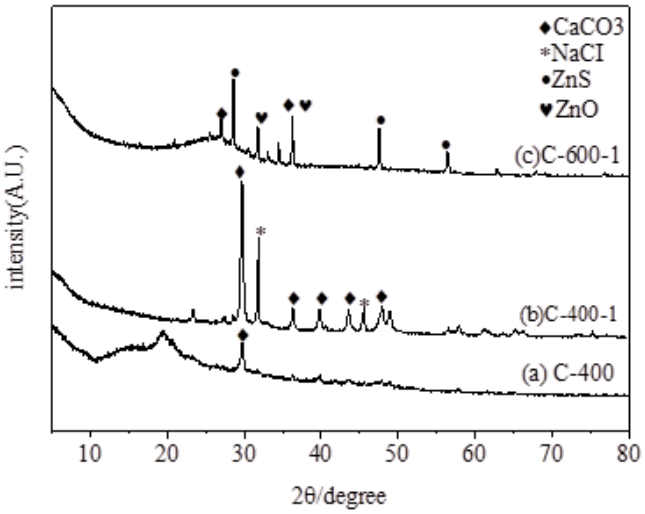


Fig. 4. XRD spectra for different samples.

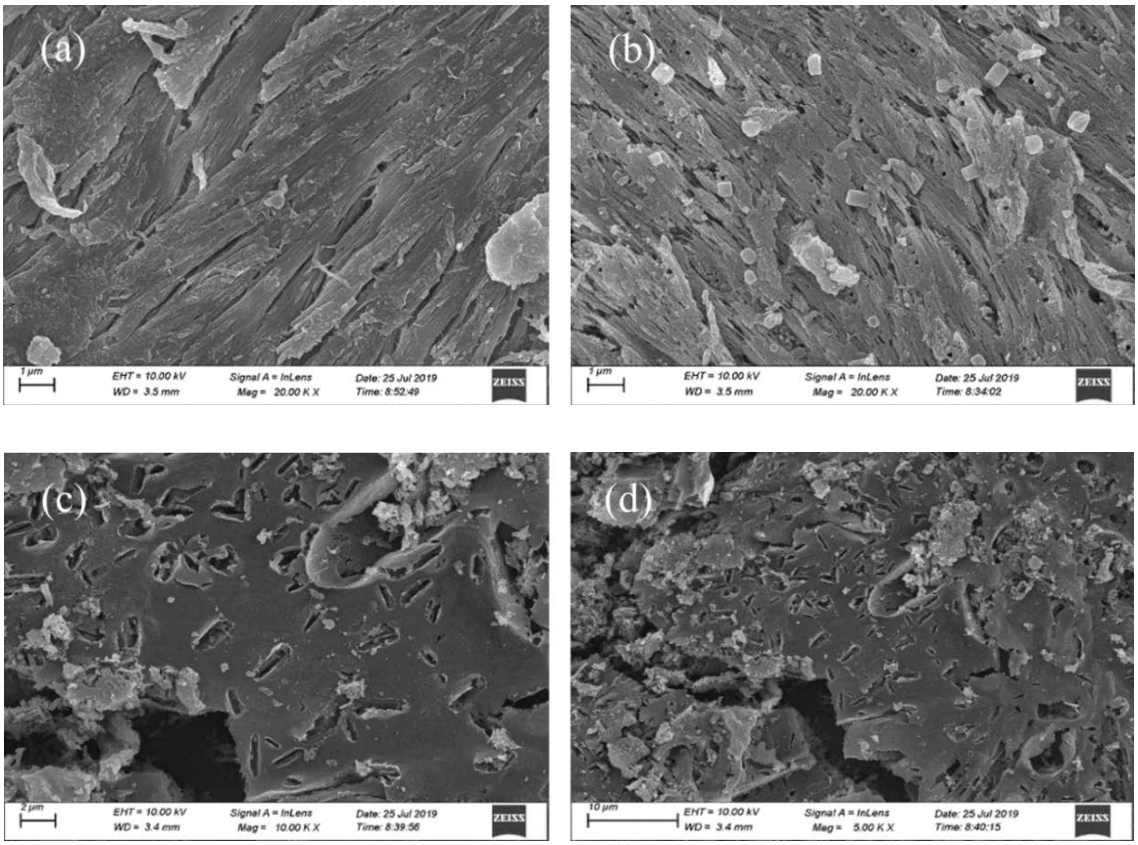


Fig. 3. Surface morphology of different samples: (a) shrimp shell, (b) C-400, (c) C400-1, and (d)C-600-1.

2θ = 29.68°($CaCO_3$), which means $CaCO_3$ in the shrimp shell carbon is the main component. The peak at the 2θ = 29.68°, 36.28°, 39.95°, 43.70°, and 47.89° represents the appearance of $CaCO_3$ in biochar activated by zinc chloride. In the XRD pattern of C-600-1, the peak at 2θ = 27.17°, 36.28°, which means that calcium carbonate appears in the activated carbon. Also, comparing the XRD patterns of C-400-1 and C-600-1, it can be found that the peak of calcium carbonate in C-600-1 is weaker than that in C-400-1, indicating that the increase in activation temperature may cause decomposition or transformation of calcium carbonate. In addition, there are peaks of zinc sulfide (2θ = 28.22°) and zinc oxide (2θ = 31.83°), this may be due to the physical and chemical process between the zinc chloride and the shrimp shell carbon during the high-temperature activation process.

### 3.2. Comparison among different carbon adsorbents

Comparison among different activated carbons was conducted to understand the co-relationship between surface properties of the carbons and their nitrate adsorption capacity. The adsorption experiments were carried by the initial nitrate concentration of 20 mg/L at pH 7.0 and the activated carbons dosage of 2.5 g/L. The results can be found in Fig. 5.

As shown by Fig. 5, the adsorption capacity of biochar for nitrate before and after activation is different, and the adsorption capacity of biochar for nitrate after activation is significantly increased. The direct pyrolyzed biochars (C400 and C600) show poor adsorption capacities towards nitrate with the final nitrate the adsorbed amount of about 0.3 mg/g (shown in Fig. 5). The activation process is confirmed to pose significant enhancement in the adsorbability. The final adsorbed amount for C-400-1, C-400-2, C-600-1, and C-600-2 are 2.4, 5.1, 3.0, and 4.2 mg/g, indicating that the activation process presents different performances at different pyrolysis temperatures. From the point of the adsorption capacity, the activation process with a $C/ZnCl_2$ ratio of 1/2 under the pyrolysis temperature of 400°C presents the highest synergistic effect in promoting the adsorption capacity. It can be seen from Table 2, the activated carbon was used in the adsorption experiment of nitrate in this study, and the maximum nitrate adsorption capacity can reach 5.58 mg/g. Compared with commercial activated carbon, it has better nitrate adsorption capacity.

In addition, it should be noticed that the adsorption capacities of the activated carbons varied according to their porous structures. So, we made a simple correlation analysis between the specific area surface and their adsorbed amount in nitrate adsorption, and the results are shown in Fig. 6. It can be seen from the figure that there is a positive linear relationship between them with a high fitting coefficient of 0.990 ($R^2$ is defined as the determination coefficient). The obtained equation is "Adsorbed amount = 0.32 + 0.0032 × $S_{BET}$". These results show that the porous structure of activated carbon determines its adsorption capacity, and the larger the surface area, the larger the adsorption capacity. Considering the similarity in the chemical composition, as well as the surficial functional groups among these activated carbons, it can be concluded that the availability of the adsorption sites might be the main limiting factor affecting the process of nitrate adsorption. Higher specific surface area means that there are more micropores, which provide more adsorption surface and adsorption sites. Thus, the adsorption capacity was enhanced. The activated carbons with relatively higher adsorption capacities (C-400-2, C-600-1, and C-600-2) were selected for subsequent study.

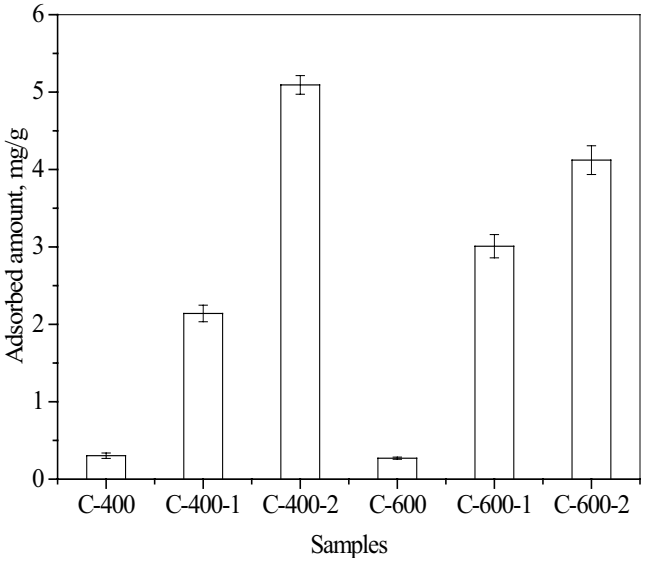


Fig. 5. Comparison among different carbon adsorbents in nitrate adsorption (adsorbent dosage = 2.5 g/L, $T$ = 298.15 K, initial nitrate concentration: 20 mg N/L, and pH = 7).

Table 2
Comparison between the synthesized adsorbents in this study and other commercial activated carbon

| Adsorbent | Adsorbate | Adsorption capacity (mg/g) | Temperature (°C) | pH | Reference |
|---|---|---|---|---|---|
| Granular chitosan | Nitrate | 2.04 | 25 | – | [39] |
| Wheat straw charcoal | Nitrate | 1.10 | 15 | – | [40] |
| Mustard straw charcoal | | 1.30 | | | |
| Commercial activated carbon (Eureka Forbes Limited, Orissa, India) | | 1.22 | | | |
| AC derived from coconut shell | Nitrate | 1.7 | 25 | 5.5 | [41] |
| C-400-2 | Nitrate | 5.58 | 25 | 3 | This study |

### 3.3. Effect of initial pH

Under different pH conditions, the adsorption capacity of activated carbon adsorbents to nitrate is different. Fig. 7 shows the influence of different initial pH on nitrate removal for different activated carbons. As shown in the figure that with the increase of acidity of the initial solution, the removal capacity of nitrate by activated carbon increases gradually, the nitrate adsorption capacity decreases as the pH value increases. Take the sample C-400-2 as an example, when the pH of the initial solution was 3.0, the adsorbed amount of nitrate in equilibrium is about 5.58 mg/g, and it decreased to 4.43 mg/g when the solution pH increased to 10.0. Since the solution is in a low pH environment, the protons in the solution neutralize the negative charge on the surface of the activated carbon. Therefore, the lower the pH value, the more positive charge sites are generated on the surface of the activated carbon, which promotes the adsorption of more nitrate ions by electrostatic attraction. When the pH increased to higher than 7.0, the surface of the activated carbon tends to negatively charge, resulting in an enhanced electrical repulsion between the activated carbon and the nitrate anions, and so the adsorption capacity was reduced. This is consistent with the findings of others [27,38].

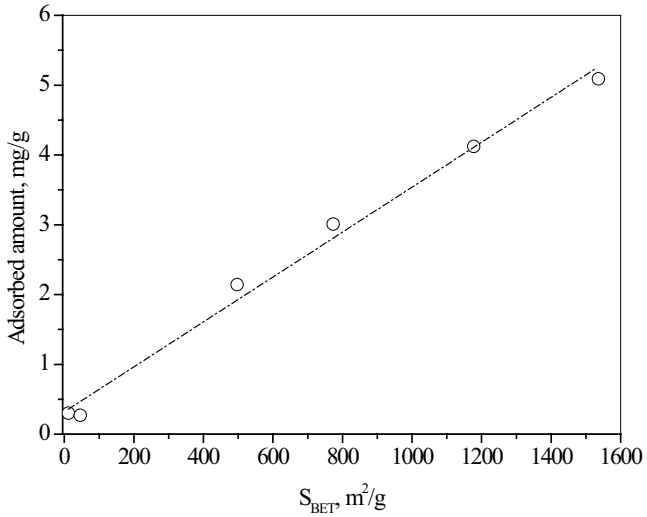


Fig. 6. Relationship between $S_{BET}$ of the activated carbons and their adsorption capacity.

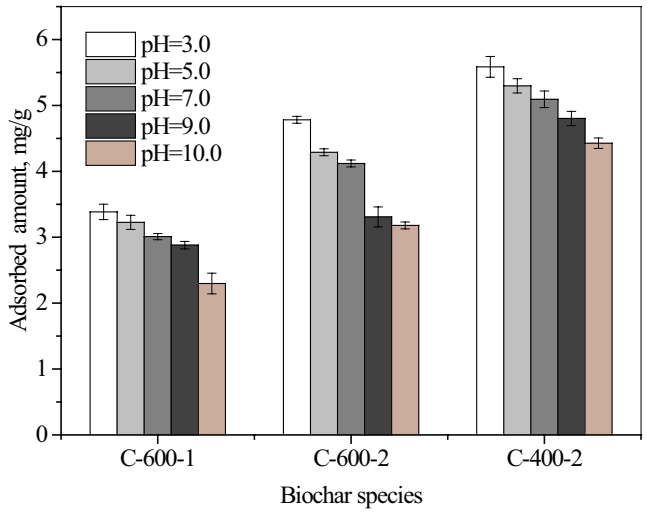


Fig. 7. Interference of initial pH on nitrate adsorption (activated carbon type: C-600-1, C-600-2, C-400-2, adsorbent dosage = 2.5 g/L, $T$ = 298.15 K, and initial nitrate concentration: 20 mg N/L).

### 3.4. Adsorption kinetics

Under different activated carbon dosages, the influence of contact time on nitrate adsorption capacity of C400-2, C600-1, and C600-2 samples are shown in Fig. 8. It can be seen from the figure that the nitrate in the solution was removed rapidly during the first 10 min adsorption. Subsequently, the adsorption process was slowed down by the instant monolayer adsorption and the rearrangement of adsorption sites on the carbon surface. Compared to the adsorption of other pollutants, the nitrate adsorption process by the activated carbon is much faster, and their equilibrium time was approximately less than 15 min. It can also be observed that the adsorbed amounts at the adsorption equilibrium decrease with the increase of the addition dosage, indicating that there is an enhanced driving force when there is a higher ratio of the target adsorbate and the adsorbent. The adsorption rate constant and equilibrium adsorption capacity of nitrate on activated carbon were studied by using a quasi-first-order equation.

The pseudo-first-order kinetic model and Avrami fractional-order models can be described as follows:

$$q_t = q_e\left(1 - e^{-k_1 t}\right) \tag{3}$$

$$q_t = q_e\left(1 - e^{-(k_3 t)n_3}\right) \tag{4}$$

where $q_t$ and $q_e$ are the amount of solute sorbed per mass of sorbent (mg/g) at any time and equilibrium, respectively, and $k_1$ is the rate constant of the pseudo-first-order model ($min^{-1}$), $k_3$ is the rate constant of the Avrami fractional-order models ($min^{-1}$), $n_3$ is the exponential of the Avrami fractional-order models.

The calculated values of the relevant parameters of the pseudo-first-order model and the Avrami fractional-order model are shown in Table 3. It can be seen that the two models fit the data well, in terms of $R^2$, the plots are found to present good correlation coefficients ($R^2$ varied from 0.967 to 0.999) with the pseudo-first-order kinetic model. This implies that the pseudo-first-order model is in good agreement with experimental data and can be used to favorably explain the adsorption process of nitrate on the selected activated carbon samples. It can be seen from Table 3, that the calculated adsorbed amounts in adsorption equilibrium ($q_e$) are quite close to the practical results, and there are significant declines in their values with the increase of the activated carbon dosage, indicating that there is a reduction in adsorption driving force induced by the increase of the adsorbent's amount. The rate constant $k_1$ presents the apparent rate in nitrate adsorption, and it

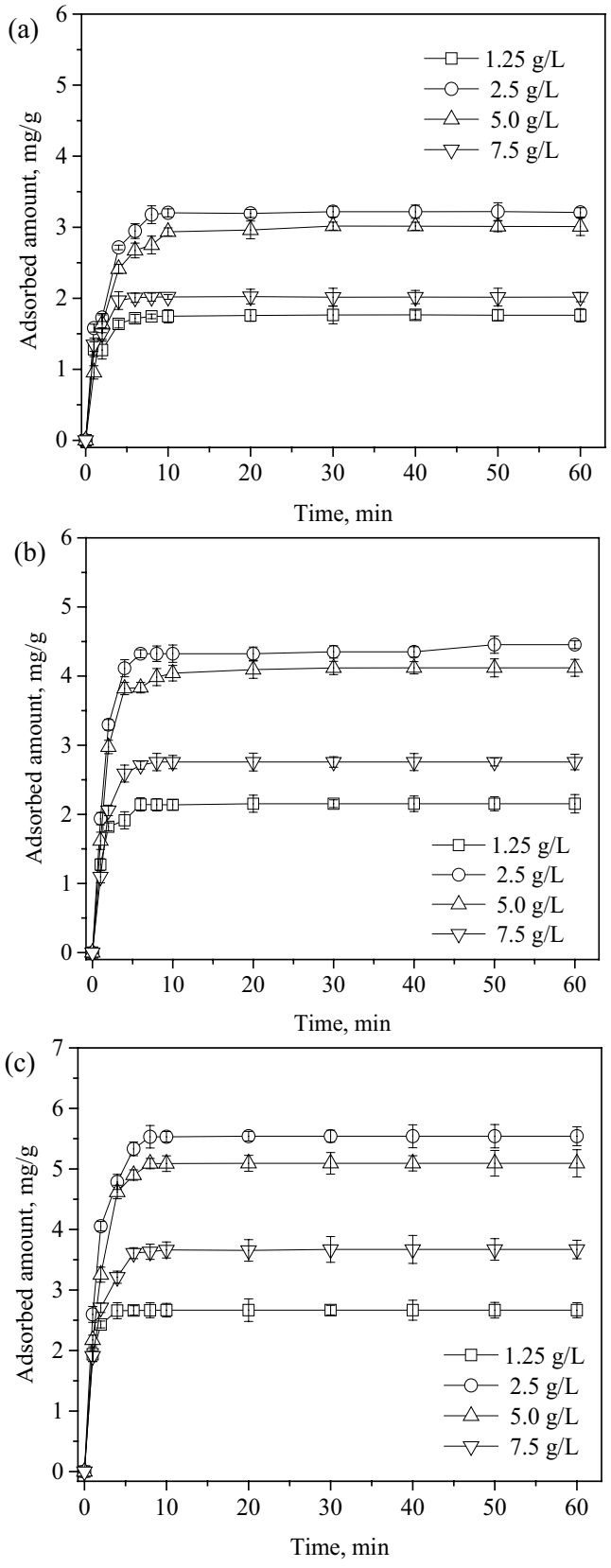


Fig. 8. Adsorption process for sample C-600-1 (a), C-600-2 (b), and C-400-2 (c) at different addition dosage. ($T$ = 298.15 K, initial nitrate concentration: 20 mg N/L, and pH = 3).

is clear that the rate constant increases with the increase of the activated carbon dosage. Take activated carbon C-600-1 as an example, the $k_1$ value increased from 0.48 to 1.0 $min^{-1}$ with the increase of the dosage from 1.25 to 7.5 g/L. Higher dosage means that more adsorbent can participate in the adsorption process and thus bring a faster removal of the nitrate in solution.

### 3.5. Adsorption isothermal

The results of the adsorption equilibrium of nitrate on different activated carbons are shown in Fig. 9. It can be seen from Fig. 9 that as the driving force of mass transfer increases when the initial concentration increases, the adsorption capacity of $q_e$ increases correspondingly with the increase of the equilibrium concentration of nitrate. The adsorption capacity of nitrate was increased from about 2.0 mg/g to about 9.0 mg/g with the increase of the equilibrium concentration from 10 to 180 mg/L. Also, we can know that the activation process greatly improves the adsorption capacity of activated carbon. The activated carbon prepared under 400°C pyrolysis with the C/$ZnCl_2$ ratio of 1/2 inactivation (C-400-2) presented the highest adsorption capacity, indicating there is an optimal activation condition.

To further explain the solid–liquid adsorption characteristics in the adsorption systems. Apply Freundlich and Langmuir isotherms to establish the correlation of equilibrium curves. The Langmuir isotherm assumes monolayer coverage on the adsorbent, while the Freundlich isotherm expresses adsorption occurs at multilayer and on energetically heterogeneous surfaces. The equations of the two models are listed as Eqs. (5)–(7):

$$\text{Langmuir model}: q_e = \frac{q_m b C_e}{1 + b C_e} \tag{5}$$

$$\text{Freundlich model}: q_e = K_f C_e^{1/n_f} \tag{6}$$

$$\text{Liu isotherm}: q_e = \frac{q_m \left(K_g C_e\right)^{n_l}}{1 + \left(K_g C_e\right)^{n_l}} \tag{7}$$

where $q_e$ (mg/g) is the nitrate uptake at equilibrium concentration $C_e$ (mg/L), $q_m$ (mg/g) is the maximum monolayer adsorption capacity, and $b$ (L/mg) is a constant in the Langmuir isothermal model related to the free energy of adsorption. $K_f$ (mg/g) $(L/mg)^{1/n}$ in the Freundlich model is the Freundlich constant related to the adsorption capacity, $K_g$ is the Liu equilibrium constant (L/mg), $n_f$ and $n_l$ are the exponents of Freundlich and Liu model, respectively (dimensionless).

The estimated model parameters with the correlation coefficient ($R^2$) are shown in Table 4. It can be seen that the experimental data are well-fitted by these models. In terms of $R^2$, both the Freundlich isothermal model, Langmuir model, and Liu model present good fitting results. From the fitting results of the experimental data to the Langmuir isothermal model, the maximum adsorption capacity ($q_m$) of nitrate by inactive biochar is about 0.625 mg/g, which

Table 3
Calculated parameters for the pseudo-first-order model

| Activated carbon | Dosage, g/L | Pseudo-first-order model | | | Avrami fractional-order models | | | |
|---|---|---|---|---|---|---|---|---|
| | | $q_e$ | $k_1$ | $R^2$ | $q_e$ | $k_3$ | $n_3$ | $R^2$ |
| C-600-1 | 1.25 | 3.2 | 0.48 | 0.982 | 1.73 | 1.001 | 1.003 | 0.959 |
| | 2.5 | 3.0 | 0.39 | 0.998 | 3.2 | 0.824 | 0.58 | 0.978 |
| | 5.0 | 2.0 | 0.91 | 0.986 | 2.98 | 0.477 | 0.819 | 0.997 |
| | 7.5 | 1.73 | 1.0 | 0.967 | 2.01 | 1.16 | 0.784 | 0.982 |
| C-600-2 | 1.25 | 4.39 | 0.65 | 0.997 | 2.13 | 1.11 | 0.805 | 0.991 |
| | 2.5 | 4.09 | 0.58 | 0.994 | 4.38 | 0.61 | 1.05 | 0.996 |
| | 5.0 | 2.77 | 0.61 | 0.995 | 4.09 | 1.06 | 0.55 | 0.993 |
| | 7.5 | 2.14 | 0.89 | 0.993 | 2.77 | 0.75 | 0.80 | 0.994 |
| C-400-2 | 1.25 | 5.52 | 0.62 | 0.997 | 2.66 | 1.29 | 0.98 | 0.998 |
| | 2.5 | 5.11 | 0.54 | 0.999 | 5.51 | 1.13 | 0.549 | 0.996 |
| | 5.0 | 3.65 | 0.68 | 0.996 | 5.10 | 0.98 | 0.54 | 0.998 |
| | 7.5 | 2.67 | 1.68 | 0.999 | 3.64 | 1.23 | 0.55 | 0.995 |

Table 4
Parameters for different isothermal models of nitrate adsorption on different activated carbons

| Adsorbent | Langmuir isothermal | | | Freundlich isothermal | | | Liu isotherm | | | |
|---|---|---|---|---|---|---|---|---|---|---|
| | $q_m$, mg/g | $b$ | $R^2$ | $K_f$ | $1/n_f$ | $R^2$ | $q_m$, mg/g | $K_g$ | $n_l$ | $R^2$ |
| C-400 | 0.625 | 0.022 | 0.988 | 2.375 | 0.006 | 0.990 | 0.734 | 0.990 | 11.844 | 0.994 |
| C-400-2 | 10.00 | 0.094 | 0.979 | 1.125 | 0.562 | 0.979 | 9.880 | 0.989 | 10.085 | 0.978 |
| C-600-1 | 8.00 | 0.035 | 0.981 | 1.750 | 0.409 | 0.980 | 9.050 | 0.978 | 13.002 | 0.964 |
| C-600-2 | 10.50 | 0.105 | 0.970 | 1.357 | 0.326 | 0.979 | 9.25 | 0.984 | 12.358 | 0.961 |

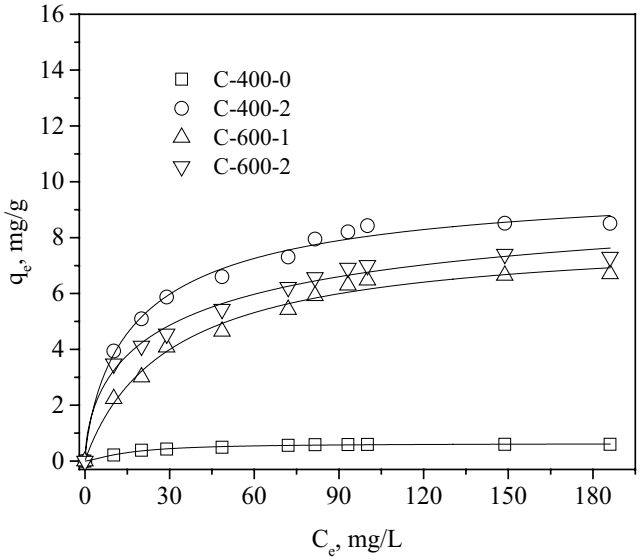


Fig. 9. The adsorption equilibrium (qe) of nitrate by different activated carbons. ($T$ = 298.15 K, adsorbent dosage = 2.5 g/L, and pH = 7).

is much lower than active carbon reported previously. The activation process promotes the adsorption capacities of the biochars, while the maximum capacities for C-400-2, C-600-1, and C-600-2 are about 10.0, 8.0, and 10.5 mg/g, respectively. The activation treatment enlarges the porous structure of the biochars and thus brings more adsorption sites to inactivated carbons' structure, which brings significant promotion in the adsorption capacity. For the Freundlich isothermal model, the constant values of $K_f$ vary from 1.125 to 1.750 for the $ZnCl_2$ activated carbons. Moreover, the constant value of $1/n_f$ in the Freundlich equation determined the type of isotherm [27]. The low value of $1/n_f$ in Table 4 indicates that there is a strong effect of bond linkage between adsorbate and absorbent. The Liu model suitably described adsorption of nitrate onto different types of activated carbon presented in Table 4. For the Liu model, the constant values of $K_g$ vary from 0.978 to 0.989 for the $ZnCl_2$ activated carbons, the constant values of $k_1$ vary from 10.085 to 13.002 for the $ZnCl_2$ activated carbons.

### 3.6. Effect of co-existing anions

In addition to the presence of nitrate in actual groundwater, there are still some anions such as sulfate, chloride, and carbonate. So, the effects of these co-existing ions on nitrate adsorption deserve study. The concentration of co-existing anions was set as 250 mg/L. Fig. 10 shows the results. It can be seen that the co-existing anions have some inhibitory effects on the adsorption of nitrate on different activated carbon. Compared with other co-existing anions,

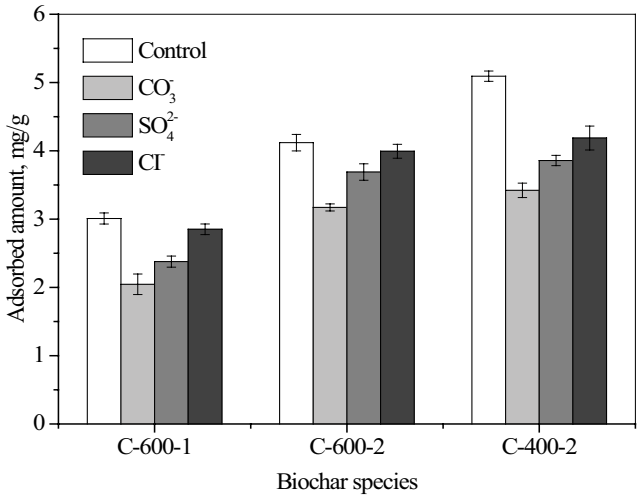


Fig. 10. Interference of various co-anions on nitrate adsorption (activated carbon type: C-600-1, C-600-2, C-400-2, adsorbent dosage = 2.5 g/L, $T$ = 298.15 K, initial nitrate concentration: 20 mg N/L, and pH = 7).

chloride had the least inhibitory effect on nitrate adsorption, followed by sulfate. The inhibitory effect of coexisting anions on the adsorption of nitrate on activated carbon is from high to low: $CO_3^{2-} > SO_4^{2-} > Cl^-$. The largest inhibitory effect of $CO_3^-$ can be ascribed to be its strong competitive with nitrate. Also, the presence of $CO_3^{2-}$ also brings a condition with higher pH values, which is confirmed to be negative for nitrate adsorption. Besides, it is reported that the monovalent anions are more difficult to be adsorbed than those with higher charge density [42]. So, the nitrate adsorption remains in the presence of $Cl^-$.

## 4. Conclusions

In this work, the activation procedure can significantly promote the specific surface area of pores and activated carbon. The increase in the impregnation ratio can obtain a higher specific surface area and pore volume, provide more positions on the adsorption of nitrate, and increase the adsorption capacity of nitrate. According to Langmuir isothermal, the maximum capacity of inactive biochar for nitrate adsorption is about 0.625 mg/g, while that for C-400-2, C-600-1, and C-600-2 are about 10.0, 8.0, and 10.5 mg/g, respectively. In a kinetic study, the nitrate in solution was rapidly removed/adsorbed during the first 10 min, and the adsorption process tends to attain an equilibrium within 50 min. The adsorption process can be well-described by pseudo-first-order kinetics. As the pH value increases, the adsorption capacity decreases gradually. Co-existing anions present some inhibition on the adsorption capacity of activated carbon for nitrate. Finally, the main advantage of this research is the realization of waste recovery from shrimp shells to adsorbents with good adsorption properties, which provides new options for carbon materials to adsorb and remove nitrates. However, there are still some points such as performance of dynamic adsorption, as well as regeneration and reusability of the adsorbents, that need further exploration.

## Acknowledgments

The authors would like to acknowledge the financial support for this work provided by the Ministry of Housing and Urban-Rural Development Science and Technology Project (2016-K6-025) and Chongqing Science and Technology Bureau Project (cstc2017shmsA20011).

## References

[1] A. Sowmya, S. Meenakshi, Zr(IV) loaded cross-linked chitosan beads with enhanced surface area for the removal of nitrate and phosphate, Int. J. Biol. Macromol., 69 (2014) 336–343.
[2] J.F. Li, Y.M. Li, Q.L. Meng, Removal of nitrate by zero-valent iron and pillared bentonite, J. Hazard. Mater., 174 (2010) 188–193.
[3] Q.Q. Zhang, J.C. Sun, J.T. Liu, G.X. Huang, C. Lu, Y. Zhang, Driving mechanism and sources of groundwater nitrate contamination in the rapidly urbanized region of south China, J. Contam. Hydrol., 182 (2015) 221–230.
[4] A. Toolabi, Z. Bonyadi, M. Paydar, A.A. Najafpoor, B. Ramavandi, Spatial distribution, occurrence, and health risk assessment of nitrate, fluoride, and arsenic in Bam groundwater resource, Iran, Groundwater Sustainable Dev., 12 (2020) 100543, doi: 10.1016/j.gsd.2020.100543.
[5] S.M. Hosseini, B. Ataie-Ashtiani, M. Kholghi, Bench-scaled nano-$Fe^0$ permeable reactive barrier for nitrate removal, Groundwater Monit. Rem., 31 (2011) 82–94.
[6] L. Fewtrell, Drinking-water nitrate, methemoglobinemia, and global burden of disease: a discussion, Environ. Health Perspect., 112 (2004) 1371–1374.
[7] P.J. Li, K.R. Lin, Z.Q. Fang, K.M. Wang, Enhanced nitrate removal by novel bimetallic Fe/Ni nanoparticles supported on biochar, J. Cleaner Prod., 151 (2017) 21–33.
[8] M. Ahmadi, A.H. Mahvi, Z. Doroud, B. Ramavandi, P. Teymouri, Kinetic and equilibrium studies on nitrate adsorption from aqueous solution by Lewatit FO 36, a resin coated with nano iron oxide, Environ. Eng. Manage. J., 15 (2016) 733–740.
[9] B. Ramavandi, S.B. Mortazavi, G. Moussavi, A. Khoshgard, M. Jahangiri, Experimental investigation of the chemical reduction of nitrate ion in aqueous solution by Mg/Cu bimetallic particles, React. Kinet. Mech. Catal., 102 (2011) 313–329.
[10] World Health Organization, Guidelines for Drinking-Water Quality, 3rd ed., WHO, Geneva, 2004.
[11] S.K. Sharma, R.C. Sobti, Nitrate removal from ground water: a review, J. Chem., 9 (2015) 1667–1675.
[12] D. Cecconet, M. Devecseri, A. Callegari, A.G. Capodaglio, Effects of process operating conditions on the autotrophic denitrification of nitrate-contaminated groundwater using bioelectrochemical systems, Sci. Total Environ., 613–614 (2017) 663–671.
[13] G.Z. Breisha, J. Winter, Bio-removal of nitrogen from wastewaters-a review, J. Am. Sci., 6 (2010) 508–528.
[14] S.B. Mortazavi, B. Ramavaandi, G. Moussavi, Chemical reduction kinetics of nitrate in aqueous solution by Mg/Cu bimetallic particles, Environ. Technol., 32 (2011) 251–260.
[15] P. Karthikeyan, H. Banu, S. Meenakshi, Synthesis and characterization of metal loaded chitosan-alginate biopolymeric hybrid beads for the efficient removal of phosphate and nitrate ions from aqueous solution, Int. J. Biol. Macromol., 130 (2019) 407–418.
[16] Y.F. Lin, H.W. Chen, Y.C. Chen, C.S. Chiou, Application of magnetite modified with polyacrylamide to adsorb phosphate in aqueous solution, J. Taiwan Inst. Chem. Eng., 44 (2013) 45–51.
[17] H.D. Raval, P.S. Rana, S. Maiti, S. Maiti, A novel high-flux, thin-film composite reverse osmosis membrane modified by chitosan for advanced water treatment, RSC Adv., 5 (2014) 6687–6694.
[18] E.M. Van Voorthuizen, A. Zwijnenburg, M. Wessling, Nutrient removal by NF and RO membranes in a decentralized sanitation system, Water Res., 39 (2005) 3657–3667.

[19] K. Tang, Y.J. Lu, L. Jiang, L.W. Wang. Y.D. Wang, A.P. Roskilly, X.L. Yu, Investigation of thermal characteristics of strontium chloride composite sorbent for sorption refrigeration, Therm. Sci. Eng. Prog., 10 (2019) 179–185.
[20] C.S. Umpierres, L.D.T. Prola, M.A. Adebayo, E.C. Lima, G.S.D. Reis, D.D.F. Kunzler, G.L. Dotto, L.T. Arenas, E.V. Benvenutti, Mesoporous $Nb_2O_5/SiO_2$ material obtained by sol–gel method and applied as adsorbent of crystal violet dye, Environ. Technol., 38 (2017) 566–578.
[21] F. Papari, P.R. Najafabadi, B. Ramavandi, Fluoride ion removal from aqueous solution, groundwater, and seawater by granular and powdered *Conocarpus erectus* biochar, Desal. Water Treat., 65 (2017) 375–386.
[22] Q.L. Hu, H.Y. Liu, Z.Y. Zhang, Y.H. Xie, Nitrate removal from aqueous solution using polyaniline modified activated carbon: optimization and characterization, J. Mol. Liq., 309 (2020) 113057, doi: 10.1016/j.molliq.2020.113057.
[23] M. Ahmadi, E. Kouhgardi, B. Ramavandi, Physico-chemical study of dew melon peel biochar for chromium attenuation from simulated and actual wastewaters, Korean J. Chem. Eng., 33 (2016) 2589–2601.
[24] M. Shahverdi, E. Kouhgardi, B. Ramavandi, Characterization, kinetic, and isotherm data for Cr(VI) removal from aqueous solution by *Populus alba* biochar modified by a cationic surfactant, Data Brief, 9 (2016) 163–168.
[25] C. Saucier, M.A. Adebayo, E.C. Lima, R. Cataluña, P.S. Thue, L.D.T. Prola, M.J. Puchana-Rosero, F.M. Machado, F.A. Pavan, G.L. Dotto, Microwave-assisted activated carbon from cocoa shell as adsorbent for removal of sodium diclofenac and nimesulide from aqueous effluents, J. Hazard. Mater., 289 (2015) 18–27.
[26] M.A. Martín-González, O. González-Díaz, P. Susial, J. Araña, J.A. Herrera-Melián, J.M. Doña-Rodríguez, Reuse of *Phoenix canariensis* palm frond mulch as biosorbent and as precursor of activated carbons for the adsorption of Imazalil in aqueous phase, Chem. Eng. J., 245 (2014) 348–358.
[27] H. Demiral, G. Gündüzoğlu, Removal of nitrate from aqueous solutions by activated carbon prepared from sugar beet bagasse, Bioresour. Technol., 101 (2010) 1675–1680.
[28] D. Angın, E. Altintig, T.E. Köse, Influence of process parameters on the surface and chemical properties of activated carbon obtained from biochar by chemical activation, Bioresour. Technol., 148 (2013) 542–549.
[29] M. Ahiduzzaman, A.K.M. Sadrul Islam, Preparation of porous biochar and activated carbon from rice husk by leaching ash and chemical activation, Springerplus, 5 (2016) 1248, doi: 10.1186/s40064-016-2932-8.
[30] G. Asimakopoulos, M. Baikousi, C. Salmas, A.B. Bourlinos, R. Zboril, M.A. Karakassides, Advanced Cr(VI) sorption properties of activated carbon produced via pyrolysis of the "*Posidonia oceanica*" seagrass, J. Hazard. Mater., 405 (2020) 124274, doi: 10.1016/j.jhazmat.2020.124274.
[31] M. Ahmadi, H. Rahmani, B. Ramavandi, B. Kakavandi, Removal of nitrate from aqueous solution using activated carbon modified with Fenton reagents, Desal. Water Treat., 76 (2017) 265–275.
[32] M.C. Ribas, M.A. Adebayo, L.D.T. Prola, E.C. Limab, R. Cataluña, L.A. Feris, M.J. Puchana-Rosero, F.M. Machado, F.A. Pavan, T. Calvete, Comparison of a homemade cocoa shell activated carbon with commercial activated carbon for the removal of reactive violet 5 dye from aqueous solutions, Chem. Eng. J., 248 (2014) 315–326.
[33] D.R. Vakilabadi, A.H. Hassani, G. Omrani, B. Ramavandi, Catalytic potential of Cu/Mg/Al-chitosan for ozonation of real landfill leachate, Process Saf. Environ. Prot., 237 (2017) 227–237.
[34] M. Ahmadi, M. Foladivanda, N. Jaafarzadeh, Z. Ramezani, B. Ramavandi, S. Jorfi, B. Kakavandi, Synthesis of chitosan zero-valent iron nanoparticles-supported for cadmium removal: characterization, optimization and modeling approach, J. Water Supply Res. Technol. AQUA, 66 (2017) 1–15.
[35] F. Yang, J. Wang, L. Liu, P. Zhang, W. Yu, Q. Deng, Z. Zeng, S. Deng, Synthesis of porous carbons with high N content from shrimp shells for efficient $CO_2$ capture and gas separation, ACS Sustainable Chem. Eng., 11 (2018) 15550–15559.
[36] G. Magnacca, F. Guerretta, A. Vizintin, P. Benzi, M.C. Valsania, R. Nisticò, Preparation, characterization and environmental/electrochemical energy storage testing of low-cost biochar from natural chitin obtained via pyrolysis at mild conditions, Appl. Surf. Sci., 427 (2018) 883–893.
[37] Y.L. Xiao, Y.W. Xue, F. Gao, A. Mosa, Sorption of heavy metal ions onto crayfish shell biochar: effect of pyrolysis temperature, pH and ionic strength, J. Taiwan Inst. Chem. Eng., 80 (2017) 114–121.
[38] S. Chatterjee, S.H. Woo, The removal of nitrate from aqueous solutions by chitosan hydrogel beads, J. Hazard. Mater., 164 (2009) 1012–1018.
[39] Q. Hu, N. Chen, C. Feng, W. Hu, Nitrate adsorption from aqueous solution using granular chitosan-$Fe^{3+}$ complex, Appl. Surf. Sci., 30 (2015) 1–9.
[40] P.C. Mishra, R.K. Patel, Use of agricultural waste for the removal of nitrate-nitrogen from aqueous medium, J. Environ. Manag., 90 (2009) 519–522.
[41] A. Bhatnagar, M. Ji, Y. Choi, W. Jung, S. Lee, S.S. Kim, G. Lee, H. Suk, H. Kim, B. Min, S.S. Kim, B. Jeon, J. Kang, Removal of nitrate from water by adsorption onto zinc chloride treated activated carbon, Sep. Sci. Technol., 43 (2008) 886–907.
[42] L.D. Hafshejania, A. Hooshmanda, A.A. Naseria, A.S. Mohammadia, F. Abbasib, A. Bhatnagar, Removal of nitrate from aqueous solution by modified sugarcane bagasse biochar, Ecol. Eng., 95 (2016) 101–111.